Desalination and Water Treatment
www.deswater.com
doi: 10.1080/19443994.2015.1055809

57 (2016) 13132–13143
June

Taylor & Francis
Taylor & Francis Group

Synthesis and physicochemical characterization of ZnMgNiAl-CO_3-layered double hydroxide and evaluation of its sodium dodecylbenzenesulfonate removal efficiency

Chafia Tiar, Mokhtar Boutahala*, Assia Benhouria, Hassina Zaghouane-Boudiaf

Laboratoire de Génie des Procédés Chimiques (LGPC), Faculté de Technologie, Université Ferhat Abbas Sétif 1, Sétif 19000, Algeria, Tel./Fax: +213 36 83 49 74; emails: chafiatiar@yahoo.fr (C. Tiar), mboutahala@yahoo.fr (M. Boutahala), assiachimie@yahoo.fr (A. Benhouria), boudiafhassina2000@yahoo.fr (H. Zaghouane-Boudiaf)

Received 14 July 2014; Accepted 21 May 2015

ABSTRACT

In this study, the adsorption of anionic surfactant by uncalcined ZnMgNiAl-CO_3 was examined using sodium dodecylbenzenesulfonate (SDBS) as a model compound in an aqueous solution. The synthesized adsorbent (ZnMgNiAl-CO_3) was characterized by FTIR, X-ray diffraction, and BET. The capacity of ZnMgNiAl-CO_3 to adsorb surfactant was evaluated at different contact times, pH values, mass effect, and initial surfactant concentrations. According to the obtained results, the adsorption processes could be described by a pseudo-second-order kinetic model. The adsorption isotherm was well fitted by the Sips model. Maximum adsorption capacity for SDBS on ZnMgNiAl-CO_3 was found to be 191.7 mg/g which was in accordance with the experimental value. Thermodynamic parameters were estimated as well, and their values indicated that the adsorption process was spontaneous and endothermic. The values of ΔH° and ΔS° of the adsorption process were 7.9 and 0.102 kJ/mol, respectively. The low value of ΔH° (<40 kJ/mol) indicated that adsorption process occurs mainly through a physical means.

Keywords: Removal; Surfactant; Sodium dodecylbenzenesulfonate (SDBS); ZnMgNiAl-CO_3

1. Introduction

Anionic surfactants such as sodium dodecylbenzenesulfonate (SDBS) are widely used in industrial processes for their favorable physicochemical properties such as detergency, foaming, emulsification, dispersion, and solubility effects [1]. These compounds are frequently found in surface and ground waters, becoming a major environmental and human health problem. For this reason, the interest in the removal of these compounds has increased and a variety of adsorbents have been investigated including layered double hydroxides (LDHs) [2].

LDHs are a family of lamellar compounds containing exchangeable anions in the interlayer space, which have the strong intralayer bonds and weak interlayer interactions [3]. Over decades, LDHs or synthetic anionic clays with a hydrotalcite-like structure have been the focus of many studies owing to their potential applications in various technologies such as ion exchangers, adsorbents, ionic conductors, catalysts, and catalyst supports [4]. Their structure consists of positively charged metal hydroxides with interlayer anions and water, with their chemical composition represented by

*Corresponding author.

the general formula: $[M^{2+}_{1-x}M^{3+}_{x}(OH)_2](A^{n-})_{X/n} \cdot mH_2O$ where M^{2+} is a bivalent cation (e.g. Ca, Mg, Zn, Co, Ni, Cu, etc.), M^{3+} is a trivalent cation (e.g. Al, Cr, Fe, Ga, Ru, Rh, etc.), and A^{n-} is a compensation anion such as Cl^-, NO_3^{2-}, ClO_4^-, CO_3^{2-} and SO_4^{2-} [5]. Based on the anionic exchange capacity and intercalation aptitudes, the LDHs are typically used as adsorbents in environmental pollution management, such as the removal of dye [6,7], chlorophenols [8,9], oxyanions [10,11], CO oxidation [12,13], sorption of metal cations [14] and surfactants [15–20].

In this study, four cations precursors were used to prepare the LDH. Isomorphic substitution of another metal improves the redox and acid–base properties of LDHs [6]. These properties are very important in catalysis and adsorption. LDHs ZnMgNiAl-CO_3 was prepared, characterized by powder X-ray diffraction (XRD), Fourier transformed infrared spectroscopy (FTIR), N_2 adsorption and used in adsorption of SDBS. In general, the calcined LDHs were used in adsorption. In this study, we used the only uncalcined sample.

2. Experimental procedures

2.1. Preparation of ZnMgNiAl-CO_3 adsorbent

ZnMgNiAl-CO_3 with $(Mg^{2+} + Ni^{2+} + Zn^{2+})/(Al^{3+})$ molar ratios of two was prepared by co-precipitation at a fixed pH 10 ± 0.5, following the method described by Reichle [21]. An aqueous solution (500 mL) containing NaOH (2 M) and Na_2CO_3 (1 M) were added dropwise to a solution (500 mL) containing $MgCl_2{\cdot}6H_2O$ (0.25 M), $AlCl_3{\cdot}6H_2O$ (0.25 M), $NiCl_2{\cdot}6H_2O$ (0.25 M), and $ZnCl_2$, $6H_2O$ (0.25 M) with vigorous stirring. The resulting slurry was aged at 65˚C for 24 h, then centrifuged, washed with deionized water until obtaining a Cl^- free ZnMgNiAl-CO_3 ($AgNO_3$ test), finally dried at 85˚C for 18 h, ground and passed through a 100-mesh sieve, giving the product ZnMgNiAl-CO_3.

2.2. Instrumentation

The distance between the layers of the ZnMgNiAl-CO_3, the basal spacing d_{003}, was determined by XRD analysis using a Bruker D8 advance diffractometer operating at 40 kV and 30 mA with Cu Kα radiation (λ = 0.15406 nm). Radial scans were recorded in the reflection scanning mode from 2θ = 2–80˚. Bragg's law, defined as $n\lambda = 2d \sin\theta$, was used to compute the crystallographic (d) for the examined LDHs samples. Nitrogen gas adsorption isotherm was measured using a Quanta Chrome Autosorb-1 instrument at 77 K. The measurements were made after degassing under vacuum at 120˚C for 12 h. The specific surface area (S.B.E.T.) was calculated by the B.E.T. method. FTIR study was carried out using FTIR 8400S Shimadzu having a standard mid-IR DTGS detector. FTIR spectra were recorded, in the range of 400–4,000 cm^{-1} with KBr pellets.

2.3. Reagent

The selected surfactant was technical grade SDBS with formula $C_{12}H_{25}C_6H_4SO_3Na$, supplied by Sigma-Aldrich. The critical micellar concentration of anionic surfactant was determined by conductance measurements. Some physical characteristics of SDBS are reported in Table 1. Reagent grade (99%) NaCl, HCl, NaOH, $AlCl_3{\cdot}6H_2O$, $NiCl_2{\cdot}6H_2O$, $ZnCl_2{\cdot}6H_2O$, Mg $Cl_2{\cdot}6H_2O$ were supplied by Sigma-Aldrich.

2.4. The determination of pHpzc

Batch equilibrium experiments were used to estimate zero point charge (pHpzc). A total of 50 mL of 0.01 M NaCl solution was poured into several erlenmeyer flasks. The pH of solution for each flask was adjusted to a value between 2 and 12 by addition of 0.1 M HCl or 0.1 M NaOH solution. Then, 50 mg of

Table 1
Some physical properties of sodium dodecyl benzene sulfonate

Chemical structure of SDBS	p*K*a	Molar mass (g/mol)	CMC in water (mg/L)	Solubility in water	Wavelength in UV (λ)
$CH_3(CH_2)_{11}C_6H_4SO_3Na$ 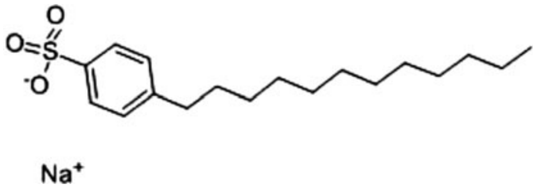	3	348.48	600	20%	222

adsorbent was added to the flasks and the dispersion was stirred for 48 h. After that time the final pH was measured. A plot of the final pH (pH_f) as a function of the initial pH (pH_i) provided pHpzc of the adsorbent by the plateau of constant pH to the ordinate.

2.5. Initial pH effect on SDBS removal

The effect of pH on adsorption of SDBS on ZnMgNiAl-CO_3 was studied. This study was conducted under an initial range of solution pH that varied from 3 to 11. The surfactant concentration in the studied solutions was 50 mg/L and the quantity of ZnMgNiAl-CO_3 was 50 mg. The volume and agitation speed were, respectively, 50 mL and 200 rpm. All studies were conducted by stirring the mixtures at 25 ± 1˚C. NaOH and HCl solutions were used to adjust the initial pH.

2.6. Effect of adsorbent dosage

The effect of adsorbent dosage on adsorption of SDBS onto ZnMgNiAl-CO_3 was conducted at pH 7 and 25 ± 1˚C for 2 h. The surfactant concentration solutions were 50 mg/L and the concentrations of ZnMgNiAl-CO_3 were 0.2–4.0 g/L.

2.7. Adsorption kinetics

Adsorption experiments were carried out in a batch equilibrium mode. For the kinetic, an amount of samples (100 mg) was dispersed in 50 mL of SDBS solution (100 mg/L) and stirred with an agitation speed of 200 rpm. After each time of contact a sample was removed and centrifuged. The SDBS concentrations were determined using UV-1700 UV spectrophotometer at 222 nm. The amount of SDBS adsorbed was derived from the initial and final concentrations of SDBS in the liquid phases. All experiments were run in triplicate to ensure reproducibility. The amount of the surfactant uptake and percentage of the removal of surfactant by the adsorbent was calculated by applying Eqs. (1) and (2), respectively:

$$q_t = \frac{C_0 - C_t}{m} V \tag{1}$$

$$\%\ \text{Removal} = 100 \frac{C_0 - C_t}{C_0} \tag{2}$$

where q_t is the amount of surfactant taken up by the adsorbent (mg/g), C_0 is the initial SDBS concentration put in contact with the adsorbent (mg/L), C_t is the surfactant concentration (mg/L) after the batch adsorption procedure, V is the volume of surfactant solution (L) put in contact with the adsorbent, and m is the mass (g) of the adsorbent.

2.8. Adsorption isotherm

For the isotherm, a constant volume of SDBS solution (50 mL) with varying initial concentrations (10–300 mg/L) were mixed with a constant amount of ZnMgNiAl-CO_3 (50 mg). The dispersions were shaken at a temperature of 25 ± 1˚C, under an agitation speed of 200 rpm. The dispersions were maintained at a constant pH 7 over 3 h to ensure the equilibrium. The SDBS q_e loading (in mg per unit weight of sample) was obtained using the following equation:

$$q_e = \frac{(C_0 - C_e) \cdot V}{m} \tag{3}$$

where C_0 and C_e (mg/L) are initial and equilibrium SDBS concentrations, respectively, V (L) is the volume of the solution, and m (g) is the adsorbent mass.

3. Results and discussion

3.1. Characterization of materials

The point of zero charge (pHpzc) of the adsorbent was determined by the pH drift method. Fig. 1 shows a plot of pH drift (pH_f) against initial pH (pH_i). The pHpzc value obtained for ZnMgNiAl-CO_3 was 8.12. Below the pHzpc, the surface of ZnMgNiAl-CO_3 was positively charged and thus effective in removing negatively charged species from aqueous solution

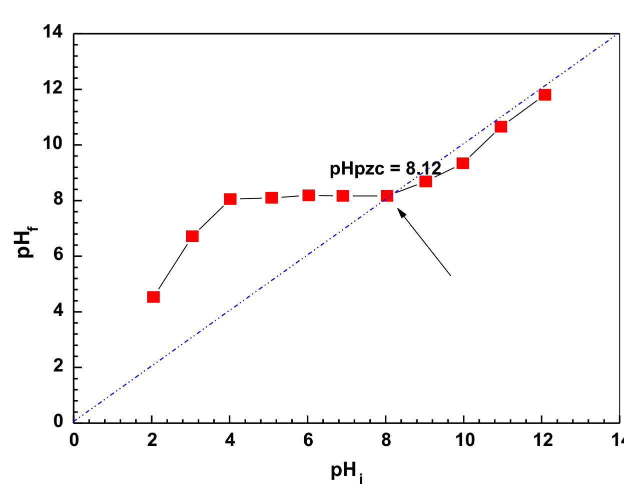

Fig. 1. Point of zero charge of ZnMgNiAl-CO_3.

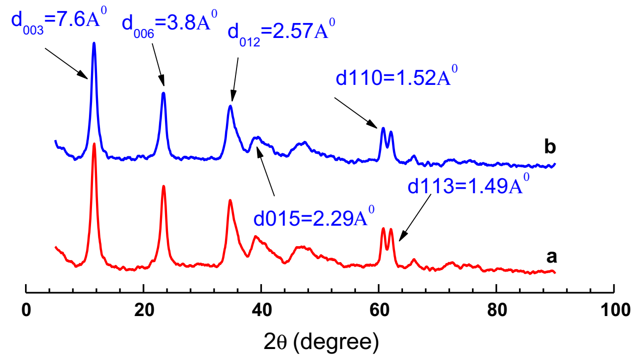

Fig. 2. Powder X-ray patterns for (a) ZnMgNi-CO_3 and (b) ZnMgNiAl-CO_3-SDBS.

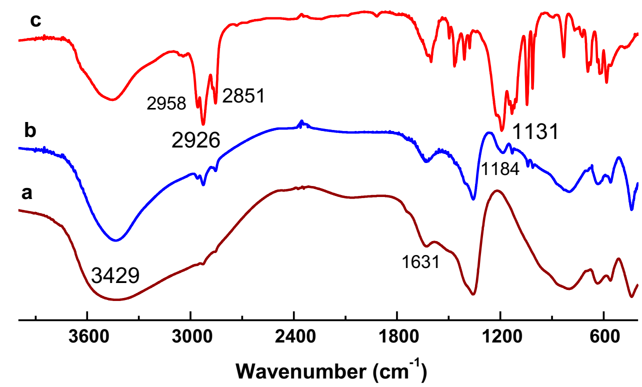

Fig. 3. FTIR spectra for (a) ZnMgNiAl-CO_3, (b) ZnMgNiAl-CO_3-SDBS, and (c) SDBS.

while at pH values above the pHzpc, the ZnMgNiAl-CO_3 surface was negatively charged.

The X-ray powder diffraction pattern of ZnMgNiAl-CO_3 is illustrated in Fig. 2(a) ZnMgNiAl-CO_3 formed a typical, well-crystallized diffraction pattern that corresponded to a hydrotalcite phase, with sharp and symmetric reflections at $2\theta = 11.61°$; 23.31°; 34.64°; 39.34°; 45.64°; 62.12°; 60.66°; those values corresponded to 7.61 Å (d_{003}), 3.82 Å (d_{006}), 2.57 Å (d_{012}), 2.29 Å (d_{015}), 1.94 Å (d_{018}), 1.52 Å (d_{110}), and 1.49 Å (d_{113}). The similar results were founded by other authors [22,23]. On the one hand, the ZnMgNiAl-CO_3 after uptake of SDBS gave a basal spacing of 7.69 Å (d_{003}) (Fig. 2(b)), which was almost the same as that of LDH precursor, but the intensity of the d_{003} peak slightly decreased, because the affinity of surfactant ion toward LDH was much lower than that of carbonate, and the ion-exchange of SDBS for carbonate in the ZnMgNiAl-CO_3 interlayer was difficult. As a result, the uptake of SDBS by ZnMgNiAl-CO_3 mainly occurs by physisorption on the surface of LDH [24].

The FTIR spectra of ZnMgNiAl-CO_3 (Fig. 3(a)) show the characteristic absorption bands of the hydrotalcite. The broad band at 3,429 cm^{-1} is due to the O–H stretching vibration of the metal hydroxide layer and interlayer water molecules. The bending vibration of the interlayer H_2O is also reflected in the broad-bands at 1,631 cm^{-1}. The strong adsorption peak at 1,360 cm^{-1} can be assigned to the vibration of the carbonate species. The band characteristic of metal–oxygen bond stretching appears below 700 cm^{-1}. The sharp bands in the 500–700 cm^{-1} range are caused by various lattice vibrations associated with metal hydroxide sheets. The adsorption of SDBS surfactant in the ZnMgNiAl-CO_3 is confirmed by the IR spectra (Fig. 3(b)) The presence of SDBS ion in the LDH is evidenced by the C–H stretching vibration bands 2,958, 2,926, and 2,821 cm^{-1}. ZnMgNiAl-CO_3-SDBS spectrum shows the stretching vibrations of the sulfonate group (1,184–1,131 cm^{-1}), C=C stretching (1,450 cm^{-1}), and the C–H bending vibrations 1,131 cm^{-1} of the benzene ring. Although, the adsorption of SDBS did not occur by interlayer anions exchange, it showed that the XRD pattern of the LDHs after adsorption experiments, (Fig. 3(b)), the d_{003} was identical to the original adsorbent but their intensity was lower. Thus, the SDBS must be only adsorbed in the surfaces of ZnMgNiAl-CO_3 LDH. The spectra of Fig. 3 are similar to those reported in the literature for the same materials [25,26].

Based on BET analysis, the specific surface area of synthetic ZnMgNiAl-CO_3 was 125.3 m^2/g. The same order of magnitude for that surface area value has been reported in the literature [5,26].

3.2. Effect of ZnMgNiAl-CO_3 dosage

The effect of ZnMgNiAl-CO_3 dosage on adsorption of SDBS is shown in Fig. 4. From Fig. 4, it followed the usual pattern of increasing removal efficiency as the adsorbent dosage increased. That corresponded to an increase in active sites for adsorption, but the value of q_e decreased. At higher adsorbent dosage, there was a very fast superficial adsorption onto the adsorbent surface that produces a lower solute concentration in the solution than when adsorbent dose was lower. Thus with increasing adsorbent dose, the amount of SDBS adsorbed per unit mass of ZnMgNiAl-CO_3 reduced, causing a decrease in q_e value. The decrease in amount of surfactant adsorbed q_e with increasing adsorbent mass was due to the split in the concentration gradient between surfactant concentration in the solution and the surfactant

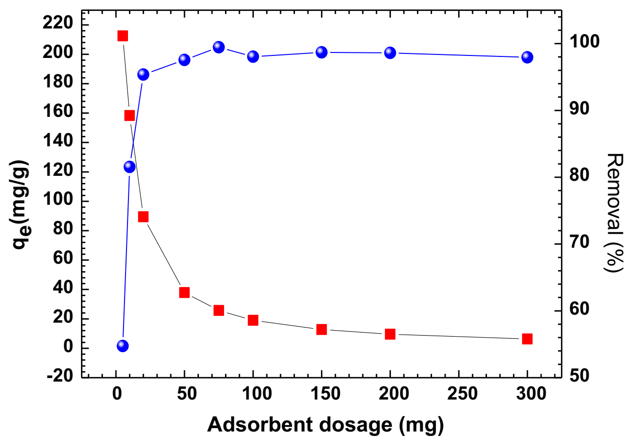

Fig. 4. Effect of the adsorbent dosage on the adsorption of SDBS onto ZnMgNiAl-CO_3.

concentration in the surface of the adsorbent. Other researches had similar results [27,28]. So the dose of 50 mg was chosen in present study.

3.3. Effect of pH on adsorption

The effect of the initial pH on adsorption provides an insight on the nature of the physicochemical interactions between the sorbate and the sorbent adsorptive sites. Generally, the initial pH of the solution can change the sorbent surface charge and the degree of ionization of the acidic sorbate molecule [2]. In our case, the sorbate molecule (SDBS) is a salt and in all pHs we have an ion $SDBS^-$. From Fig. 5, the SDBS removal efficiency slightly changed when the pH values changed from 2 to 7, indicating that the binding affinity between SDBS and the binding sites did not significantly change under acidic conditions. The maximum SDBS removal efficiency was reached within the pH range of 6–8, with its value fluctuating between 91 and 89%. The removal efficiencies of ZnMgNiAl-CO_3 clearly decreased when the pH was increased above 8. A similar behavior was observed in other adsorbents, such as activated carbon [29], mineral oxides, and clays [30]. The adsorption was favorable in acidic medium. This phenomena was due to the strong interaction between anionic SDBS and positively adsorbent surface charge (pHsol < pHpzc). At basic pH, the SDBS uptake was lower due to the electrostatic repulsions between the negative surface charge (pHpzc < pH (solution)) and the SDBS anions. Besides, there might be competition between the OH^- ions in the solution and the SDBS anions [6]. So the pH of SDBS solution (near 7) was not adjusted in the next experiments.

3.4. Effect of contact time and initial SDBS concentration

The effect of contact time on adsorption capacity of ZnMgNiAl-CO_3 for SDBS at different initial SDBS concentrations is shown in Fig. 6. This figure shows that the adsorption capacity increases with the increase in contact time, and the adsorption reached equilibrium in about 250 min (4.10 h). An adsorption capacity of 220 mg/g is obtained at 4.1 h contact time, 400 mg/L initial concentration, pH 7, and 1 g/L adsorbent dose. This figure also shows that rapid increase in adsorption of SDBS achieved during the first 1 h. The fast

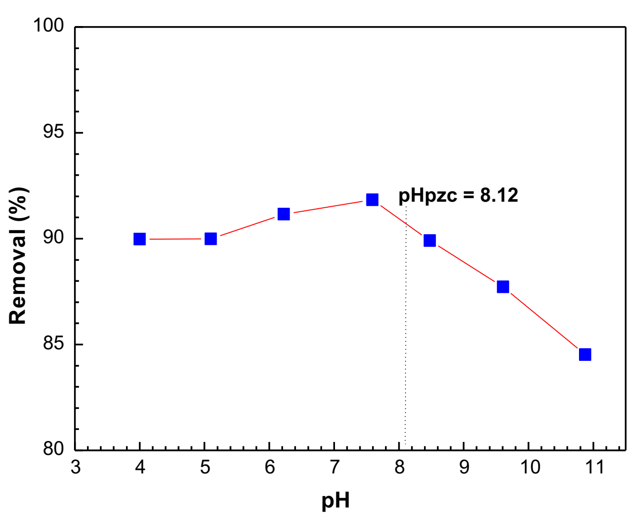

Fig. 5. Effect of initial pH on adsorption of SDBS onto ZnMgNiAl-CO_3 sample.

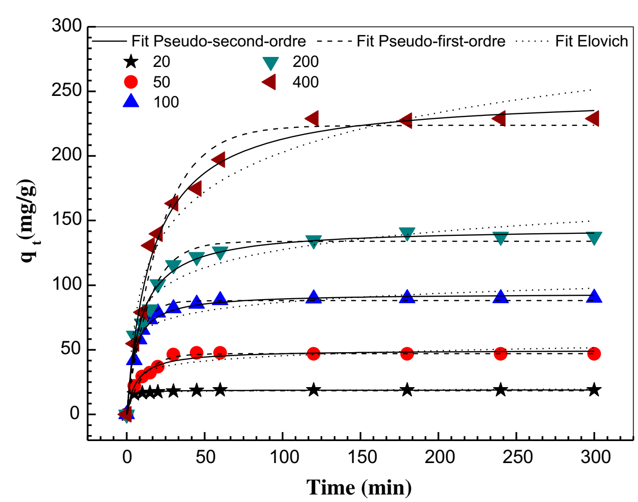

Fig. 6. Effect of contact time and initial SDBS concentrations.

adsorption at the initial stage may be due to the higher driving force making fast transfer of SDBS ions to the surface of ZnMgNiAl-CO_3 particles and the availability of the uncovered surface area and the remaining active sites on the adsorbent [31].

3.5. Adsorption kinetics

Generally, three steps are involved during the process of adsorption by porous adsorbent particles: external mass transfer, intraparticle transport, and chemisorption [32].

To investigate the mechanism of surfactant adsorption, three kinetic models were considered, pseudo-first-order, pseudo-second-order, and the Elovich equation. Those models were the most commonly used to describe the adsorption of dyes, organic and inorganic pollutants onto solid adsorbents [33]. There is no study about kinetic modeling of adsorption of SDBS from aqueous solution onto ZnMgNiAl-CO_3. In this work, adsorption kinetics of SDBS onto ZnMgNiAl-CO_3 was studied in terms of the Lagergren pseudo-first-order model (Eq. (4)) [34], Ho' pseudo-second-order model (Eq. (5)) [35], and Elovich model (Eq. (6)) [36].

$$\ln (q_t - q_e) = \ln (q_e) - K_1 t \tag{4}$$

$$1/q_e = 1K_2 q_e^2 + (1/q_e)t \tag{5}$$

$$q_t = \frac{1}{\beta} \ln (\alpha \times \beta) + \frac{1}{\beta} \ln (t) \tag{6}$$

where q_e and q_t are the amount of SDBS adsorbed (mg/g) onto adsorbent at the equilibrium time and at time t (min), respectively. Values of K_1 (L/min) and K_2 (g/mg min) were calculated from the plot of ln $(q_e - q_t)$ vs. t and t/q_t vs. t, respectively. α is the initial adsorption rate (mg/g min), β is the desorption constant (g/mg). Besides the value of R^2, the applicability of the kinetic models to describe the adsorption process was further validated by the normalized standard deviation, Δq (%), which is defined as:

$$\Delta q\ (\%) = 100\sqrt{\frac{\Sigma[(q_{\exp} - q_{\text{cal}})/q_{\text{ex}}]^2}{N-1}} \tag{7}$$

where N is the number of data points, $q_{\exp}$ and q_{cal} (mg/g) are the experimental and calculated adsorption capacities, respectively.

The calculated constants of the three kinetic equations along with R^2 values at different initial SDBS concentrations are presented in Table 2. The linear plots of ln $(q_e - q_t)$ vs. t and q_t vs. $\ln(t)$ for

Table 2
The kinetic parameters evaluated for SDBS adsorption by ZnMgNiAl-CO_3

Models	Parameters	Initial concentration				
		20	50	100	200	400
First-order kinetic model:	K_1	0.0317	0.0463	0.0398	0.0308	0.0301
$\ln (q_t - q_e) = \ln (q_e) - K_1 t$	ln q_e (cal)	3.5	19.9	35.7	84.9	178.8
	R^2	0.82	0.875	0.946	0.933	0.929
	Δq (%)	0.852	1.141	0.535	0.309	0.482
Second-order kinetic model:	K_2	0.0347	0.00553	0.003	0.00087	0.000267
$1/q_e = 1/K_2 q_e^2 + (1/q_e)t$	q_e (cal)	19.04	47.64	91.24	142.65	243.9
	h	12.58	12.55	24.974	17.7	15.88
	R^2	0.999	0.999	0.999	0.999	0.998
	Δq (%)	0.021	0.057	0.012	0.018	0.015
Elovich:	B	1.61	0.179	0.1021	0.0494	0.0227
$q_t = \frac{1}{\beta}\ln(\alpha \times \beta) + \frac{1}{\beta}\ln(t)$	R^2	0.61146	0.669	0.7568	0.893	0.9274
	Δq (%)	0.652	5.185	7.611	9.4339	16.689
Intraparticle diffusion:	K_3	0.015	0.037	0.743	1.536	0.313
$q_t = K_3\sqrt{t} + C$	C	18.7	46.3	79.12	114.85	223.68
	R^2	0.909	0.81	0.646	0.705	0.73
	Δq (%)	0.018	0.081	2.557	4.040	0.491
Experimental date		17.85	46.2	90.08	138.01	227.7

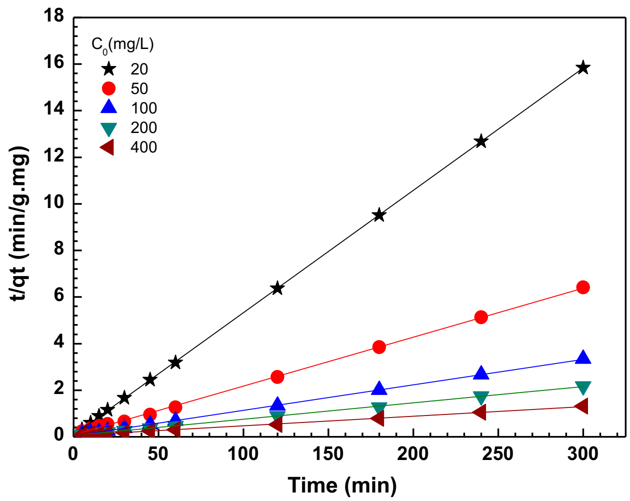

Fig. 7. Pseudo-second-order kinetic plot for the adsorption of SDBS onto ZnMgNiAl-CO_3.

pseudo-first-order and Elovich equations, respectively, (figures not shown) are of low R^2 values, as shown in Table 2. Moreover, this table shows a large difference between the experimental and calculated adsorption capacity values Δq(%), indicating a poor pseudo-first order and Elovich fit to the experimental data. High R^2 values are obtained for the linear plot of t/q_t vs. t (Fig. 7) for pseudo-second-order equation, as shown in Table 2. It can be seen that the pseudo-second-order kinetic model better represented the adsorption kinetics and there are well agreements between the experimental and calculated adsorption capacity values Δq (%) (Table 2). This suggests that the adsorption of SDBS on ZnMgNiAl-CO_3 follows second-order kinetics. A similar result was reported by Taffarel and Rubio [37] for the adsorption of SDBS on modified natural zeolite with CTAB. From Fig. 6, nonlinear forms of pseudo-second-order kinetic model studied at different conditions also showed the better fit than pseudo-first-order and Elovich kinetic model, indicating the adsorption of SDBS was due to chemisorption. Also from Fig. 6, the results suggested that pseudo-first-order and Elovich models would be applicable only over the initial stage of the adsorption process. The values of rate constant K_2 decrease with increasing initial concentration of SDBS. The reason for that behavior could be attributed to the high competition for the adsorption surface sites at high concentration which led to higher sorption rates. The initial adsorption rates can be calculated from the pseudo-second-order model by the following equation: $h = K_2 q_e^2$, and the results are shown in Table 2. The result noticed that initial adsorption rate increased with elevating the initial SDBS concentration and maximum value was obtained at 100 mg/L concentration and then decreased after that.

3.6. Adsorption mechanism

Adsorption kinetics is usually controlled by different mechanisms. The intraparticle diffusion theory [38] is derived from Fick's law assumes that the diffusion of the liquid film surrounding the adsorbent is negligible, and intraparticle diffusion is the only rate controlling step of the adsorption process. Eq. (8) shows the mathematical expression used to study this phenomenon.

$$q_t = K_3\sqrt{t} + C \quad (8)$$

where K_3 (mg/g min$^{1/2}$) is the intraparticle diffusion rate constant and C is the value of the intercept of the plot of q_t against $t^{1/2}$.

The pseudo-first-order and pseudo-second-order kinetic model cannot identify the diffusion mechanism, and then the kinetic data were analyzed by using the intraparticle diffusion model. According to this model, the plot of uptake q_t, vs. the square root of time, $t^{1/2}$, should be linear if the intraparticle diffusion is involved in the adsorption, and if these lines pass through the origin, then intraparticle diffusion is the rate controlling step, otherwise this indicates that two or more steps occur in the adsorption process. The plots shown in Fig. 8 presented multilinearity, indicating that three steps took place. As can be seen in

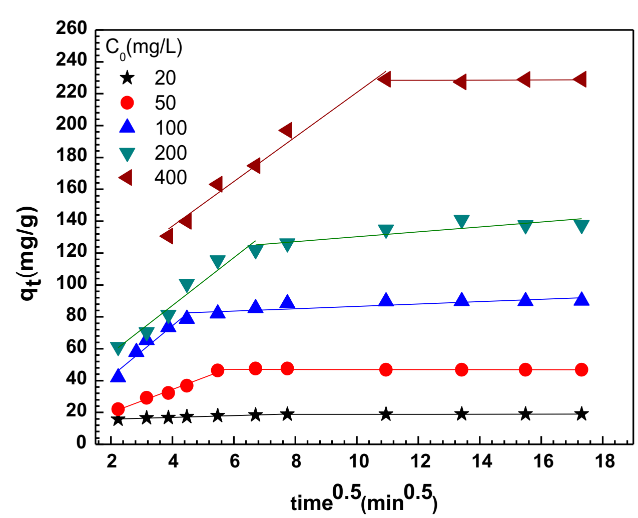

Fig. 8. The Weber–Morris plot of the kinetic data for SDBS adsorption onto ZnMgNiAl-CO_3 at different concentrations.

Fig. 8, the first sharper step was not observed and completed before 10 min, which may be considered as the external surface adsorption. The second step described the gradual adsorption from 10 to 50 min, where intraparticle diffusion was rate controlling. The third step was attributed to the final equilibrium stage, in which intraparticle diffusion started to slow down due to the decrease in SDBS concentration in solution. The slope of the second step characterized the rate parameter corresponding to the intraparticle diffusion, and the intercept was proportional to the boundary layer thickness. Fig. 8 also shows the linear plots of the second and the third stages did not pass through the origin. It shows that intraparticle diffusion was not the only rate limiting mechanism in the adsorption process. Some other mechanism along with intraparticle diffusion is also involved.

The R^2 values (Table 2) for this model were lower compared to those obtained from pseudo-first-order, pseudo-second-order and Elovich models. Also, there was high deviation between the calculated and experimental values Δq (%). The C intercept values gave an idea of the boundary layer thickness, i.e. the larger the intercept, the greater the effect of the boundary layer. The values of intercept C (Table 2) provide information about the thickness of the boundary layer and the external mass transfer resistance. The constant C was found to increase from 18.7 to 223.7 with increase in SDBS amount from 50 to 400 mg/L. The intraparticle diffusion rate constant, K_3 value was in the range of 0.015–1.536 mg/g min$^{1/2}$.

3.7. Adsorption isotherm

Adsorption isotherm can describe how adsorbates interact with adsorbents in an adsorption system. Adsorption isotherm for surfactant retention by ZnMgNiAl-CO_3 is presented in Fig. 9. This isotherm indicates that surfactant has a high affinity for ZnMgNiAl-CO_3 surface, particularly at low surfactant concentrations. Isotherm was a characteristic of typical L-type adsorption reaction that represented a system where the adsorbate was strongly attracted by the adsorbent, generally by ion–ion exchange interactions that reached a saturation value represented by "the plateau" of the isotherm [39]. The L-type ion-exchange isotherms have been reported by other authors for the adsorption of many organic [7,8], inorganic [40–42], dyes [43,44], and surfactant [45] anions on LDHs. The analysis requires equilibrium to better understand the adsorption process. In this paper, the Langmuir, Freundlich, Sips, and Toth models were applied and the nonlinear equations were listed as following.

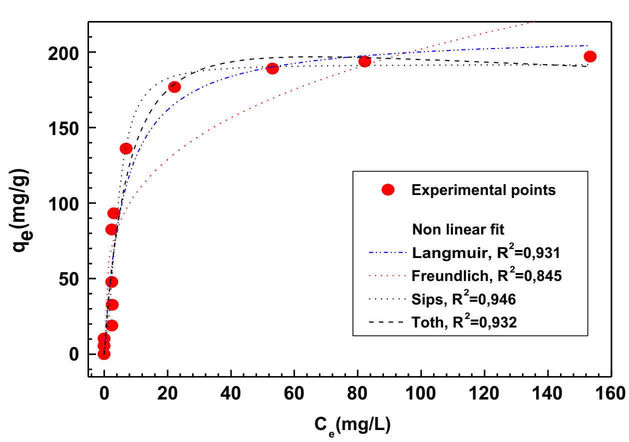

Fig. 9. SDBS adsorption isotherm onto ZnMgNiAl-CO_3.

3.7.1. Langmuir isotherm

The Langmuir adsorption isotherm has been successfully applied to many pollutant adsorption processes and has been the most widely used sorption isotherm for the sorption of a solute from a liquid solution [46]. The saturated monolayer isotherm can be represented as:

$$q_e = \frac{q_m K_L C_e}{1 + K_L C_e} \tag{9}$$

For the Langmuir isotherm, an equilibrium parameter, R_L, is the essential characteristics of this isotherm, which can be expressed as follows:

$$R_L = \frac{1}{1 + K_L C_0} \tag{10}$$

where C_e is the equilibrium concentration (mg/L), q_e is the amount of SDBS adsorbed onto ZnMgNiAl-CO_3 (mg/g), q_m is q_e for a complete monolayer (mg/g), a constant related to sorption capacity, and K_L is a constant related to the affinity of the binding sites and energy of adsorption (L/mg). C_0 is the highest initial solute concentration, and R_L indicates the type of isotherm to be reversible ($R_L = 0$), favorable ($0 < R_L < 1$), linear ($R_L = 1$), or unfavorable ($R_L > 1$).c

3.7.2. Freundlich isotherm

Freundlich isotherm is an empirical equation describing adsorption onto a heterogeneous surface. The Freundlich isotherm is commonly presented as:

$$q_e = K_F C_e^{1/n} \quad (11)$$

where K_F and n are the Freundlich constants related to the adsorption capacity and adsorption intensity of the adsorbent, respectively [47].

3.7.3. Sips isotherm

The Sips isotherm is a combination of Langmuir and Freundlich isotherms; it suggests that the equilibrium data follow the Freundlich curve at lower initial solute concentration, but it follows the Langmuir trend at higher solute concentration [48]. It is given as:

$$q_e = \frac{q_S K_S C_e^{1/m}}{1 + K_S C_e^{1/m}} \quad (12)$$

where q_e is the solid phase sorbate concentration in equilibrium (mg/g), C_e is the liquid phase sorbate concentration in equilibrium (mg/L), q_S (mg/g) is the Sips maximum uptake of SDBS per unit mass of ZnMgNiAl-CO_3, K_S (L/mg), $1/m$ is the Sips constant related to energy of adsorption, parameter m could be regarded as the Sips parameter characterizing the system heterogeneity, C_0 is the highest initial solute concentration (L/g).

3.7.4. Toth isotherm

The Toth model is an improvement of the Freundlich and Langmuir equations [31]. The equation describes well the adsorption behavior under subcritical conditions of several adsorbates.

$$q_e = \frac{q_r K_T C_e}{[1 + (K_T C_e)^{m_T}]^{1/m_T}} \quad (13)$$

where q_e (mg/g) is the equilibrium amount of adsorbate by the solid, C_e (mg/L) is the equilibrium concentration of adsorbate, q_T (mg/g) and K_T (L/mg) are the Toth constants, representing the monolayer adsorption capacity and the energy of adsorption, respectively, and m_T is an empirical constant.

Nonlinear regression is used to determine the best-fitting isotherm, and the applicability of isotherm equations is compared by judging the correlation coefficients R^2. The calculated constants of the four isotherm equations along with R^2 values are presented in Table 3. This table shows that the Sips isotherm gave the best correlation with R^2 value of 0.937 at 25°C. This may due to the ability of Sips isotherm to predict wide adsorbate concentration ranges. From Table 3, it can be noticed that for the Langmuir isotherm, the value of R_L is 0.018 for temperature of 398 K, indicate the favorability of SDBS adsorption on ZnMgNiAl-CO_3. The results of Table 3 show that the Langmuir isotherm correlates the data with R^2 value higher than that of Freundlich and Toth isotherm, which reflects the monolayer adsorption. In this study, maximum SDBS adsorption capacity of 191.7 mg/g is

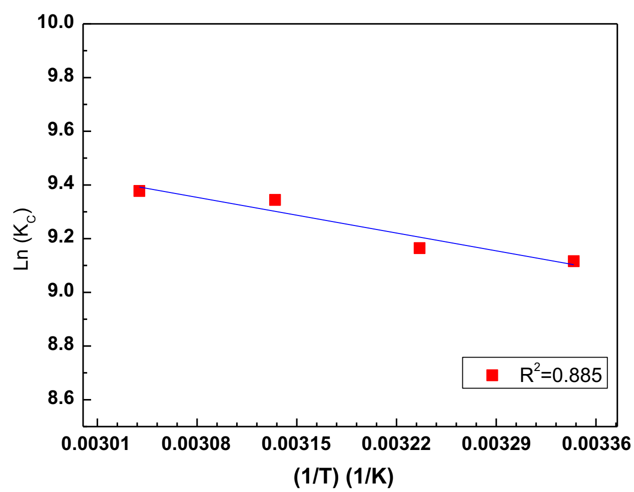

Fig. 10. Van't Hoff plot for the adsorption of SDBS onto ZnMgNiAl-CO_3.

Table 3
Freundlich, Langmuir, Sips, and Toth parameters for the SDBS adsorption

Langmuir		Freundlich		Sips		Toth	
q_m (mg/g)	212.6			q_m (mg/g)	191.7	q_m (mg/g)	246.9
K_L	0.16	K_F	55.86	K_S	0.063	K_T (dm^3/mg)	0.102
R_L	0.018	n	3.58	M	0.521	m_T	1.12
R^2	0.931	R^2	0.845	R^2	0.946	R^2	0.932
Δq (%)	21.52	Δq (%)	32.29	Δq (%)	19.1	Δq (%)	21.41

Table 4
Thermodynamics adsorption parameters for SDBS on ZnMgNiAl-CO_3

		ΔG (kJ/mol)			
ΔH (kJ/mol)	ΔS (kJ/mol)	299	309	319	329
7.8	0.102	−22.64	−23.66	−24.69	−25.71

reported (Table 3), as calculated from Sips isotherm fitting, which is in accordance with the experimental value.

3.8. Adsorption thermodynamics

The thermodynamic parameters such as change in Gibbs free energy (ΔG°), enthalpy (ΔH°), and entropy (ΔS°) were estimated to evaluate the feasibility and nature of the adsorption reaction. Experiments were carried out using 50 mg/L of SDBS solutions and 50 mg of adsorbent ZnMgNiAl-CO_3 at temperatures 26, 36, 46, and 56 ± 1˚C. The Gibbs free energy change of the process is related to the equilibrium constant ($K_C = (1{,}000\ q_e/C_e)$ by the following equation (Eq. (14)) [49,50].

$$\Delta G^\circ = -RT \ln K_C \tag{14}$$

From thermodynamics, the Gibbs free energy change is also related to enthalpy change and entropy change at constant temperature by the following equation (Eq. (15)).

$$\Delta G^\circ = \Delta H^\circ - T\Delta S^\circ \tag{15}$$

The values of ΔH° and ΔS° were calculated from the slope and intercept of the plots of $\ln K_d$ vs. $1/T$ (Fig. 10). The calculated values of ΔH°, ΔS°, and ΔG° are listed in Table 4. The obtained values for Gibbs free energy change ΔG° are −22.64, −23.66, −24.69, and −25.71 kJ/mol for SDBS adsorption on ZnMgNiAl-CO_3 at 299, 309, 319, and 329 K, respectively. The negative ΔG° values indicate thermodynamically spontaneous nature of the adsorption. The positive enthalpy change (ΔH°) values for the SDBS adsorption reaction indicate the endothermic nature of the present reaction. Low positive enthalpy change ($\Delta H^\circ < 40$ kJ/mol) also indicated the physical sorption of SDBS onto ZnMgNiAl-CO_3 surface. The positive entropy change (ΔS°) for this reaction (Table 4) has also indicated the increase in number of species at the solid–liquid interface and hence the randomness in the interface which is presumably due to the release of aqua molecules when the aquated SDBS is adsorbed on the surface of the adsorbent.

Table 5
Adsorption capacities of different adsorbents used for removal of SDBS

Adsorbent	q_{max} (mg g^{-1})	References
Activated carbons	260–470	[51]
Organophilic bentonite	150	[52]
Alumina	19.8	[53]
Modified natural zeolithe	30.7	[37]
PANI doped with $CuCl_2$	32.3	[54]
PANI doped with $ZnCl_2$	29.5	[54]
Zn–Mg–Ni–Al–CO_3	191.7	This study

4. Conclusion

The results obtained in this study suggest that ZnMgNiAl-CO_3 is very efficient sorbent for anionic surfactant and showed a higher adsorption capacity toward SDBS at low concentrations. Three adsorption kinetic models were tested and the pseudo-second-order model fit the experimental data well. The intraparticle diffusion study yielded two or three linear regions, which suggested that surfactant adsorption involves more than one kinetic stage. The Sips model fit the experimental data well, suggesting that the adsorption occurs in a monolayer. The maximum adsorption capacity for the adsorption of SDBS onto ZnMgNiAl-CO_3 was found to be 191.7 mg/g. The negative value of ΔG° at different temperatures indicated spontaneity and the positive value of ΔH° showed the endothermic nature of SDBS adsorption. Comparing our prepared uncalcined LDHs with other low-cost adsorbents (Table 5), we think that the material is very competitive. The best-fit adsorption isotherm was achieved with this material particularly promising for the removal of anionic surfactant in industrial wastewater treatment.

References

[1] A. Ourari, A. Flilissa, M. Boutahala, HocineIlikti, Removal of cetylpyridinium bromide by adsorption onto maghnite: Application to paper deinking, J. Surfact. Deterg. 17 (2014) 785–793.

[2] M. José dos Reis, F. Silvério, J. Tronto, J.B. Valim, Effects of pH, temperature, and ionic strength on adsorption of sodium dodecylbenzenesulfonate into Mg–Al–CO_3 layered double hydroxides, J. Phys. Chem. Solids 65 (2004) 487–492.

[3] T. Zhang, Q. Li, H. Xiao, Z. Mei, H. Lu, Y. Zhou, Enhanced fluoride removal from water by non-thermal plasma modified CeO_2 Mg–Fe layered double hydroxides, Appl. Clay Sci. 72 (2013) 117–123.

[4] D.S. Tong, C.H. Zhou, M.Y. Li, W.H. Yu, J. Beltramini, C.X. Lin, Z.P. Xu, Structure and catalytic properties of Sn-containing layered double hydroxides synthesized in the presence of dodecylsulfate and dodecylamine, Appl. Clay Sci. 48 (2010) 569–574.

[5] F. Cavani, F. Trifirò, A. Vaccari, Hydrotalcite-type anionic clays: Preparation, properties and applications, Catal. Today 11(2) (1991) 173–301.

[6] H. Zaghouane-Boudiaf, M. Boutahala, L. Arab, Removal of methyl orange from aqueous solution by uncalcined and calcined MgNiAl layered double hydroxides (LDHs), J. Chem. Eng. 187 (2012) 142–149.

[7] N.D. Setti, N. Jouini, Z. Derriche, Sorption study of an anionic dye-benzopurpurine 4B-on calcined and uncalcined Mg–Al layered double hydroxides, J. Phys. Chem. Solids 71 (2010) 556–559.

[8] H. Zaghouane-Boudiaf, M. Boutahala, C. Tiar, L. Arab, F. Garin, Treatment of 2,4,5-trichlorophenol by MgAl–SDBS organo-layered double hydroxides: Kinetic and equilibrium studies, J. Chem. Eng. 173 (2011) 36–41.

[9] S.L. Chen, Z.P. Xu, Q. Zhang, C.Q. Max Lu, Z.P. Hao, S.M. Liu, Studies on adsorption of phenol and 4-nitrophenol on MgAl-mixed derived from MgAl-layered double hydroxide, Sep. Purif. Technol. 67 (2009) 194–200.

[10] L. Arab, M. Boutahala, B. Djellouli, Étude de l'élimination du Cr(VI) par l'oxyde mixte obtenu par calcination de l'hydroxyde double lamellaire MgAl, C.R. Chim. 17 (2014) 860–868.

[11] Y. Guo, Z. Zhu, Y. Qiu, J. Zhao, Synthesis of mesoporous Cu/Mg/Fe layered double hydroxide and its adsorption performance for arsenate in aqueous solutions, J. Environ. Sci. 25(5) (2013) 944–953.

[12] L. Arab, M. Boutahala, B. Djellouli, Thierry Dintzer, Veronique Pitchon, Characteristics of gold supported on nickel-containing hydrotalcite catalysts in CO oxidation, Appl. Catal., A 475 (2014) 446–460.

[13] L. Li, Q. Chen, Q. Zhang, J. Shi, Y. Li, W. Zhao, J. Shi, Layered double hydroxide confined Au colloids: High performance catalysts for low temperature CO oxidation, Catal. Commun. 26 (2012) 15–18.

[14] X. Liang, Y. Zang, Y. Xu, X. Tan, W. Hou, L. Wang, Y. Sun, Sorption of metal cations on layered double hydroxides, Colloids Surf., A 433 (2013) 122–131.

[15] P.C. Pavan, E.L. Crepaldi, G.A. de A. Gomes, J.B. Valim, Adsorption of sodium dodecylsulfate on a hydrotalcite-like compound. Effect of temperature, pH and ionic strength, Colloids Surf., A 154 (1999) 399–410.

[16] P.C. Pavan, E.L. Crepaldi, J.B. Valim, Sorption of anionic surfactants on layered double hydroxides, J. Colloid Interface Sci. 229 (2000) 346–352.

[17] M. José dos Reis, F. Silvério, J. Tronto, J.B. Valim, Effects of pH, temperature, and ionic strength on adsorption of sodium dodecylbenzenesulfonate into Mg–Al–CO_3 layered double hydroxides, J. Phys. Chem. Solids 65 (2004) 487–492.

[18] H. Zhang, X. Wen, Y. Wang, Synthesis and characterization of sulfate and dodecyl benzenesulfonate intercaled zinc–iron layered double hydroxides by one-step coprecipitation, J. Solid State Chem. 180 (2007) 1636–1647.

[19] F.R. Costa, A. Leuteritz, U. Wagenknecht, D. Jehnichen, L. Häußler, G. Heinrich, Intercalation of Mg–Al layered double hydroxide by anionic surfactants: Preparation and characterization, Appl. Clay Sci. 38 (2008) 153–164.

[20] M. Bouraada, M. Lafjah, M. Ouali, L. Demenorval, Basic dye removal from aqueous solutions by dodecylsulfate- and dodecyl-benzene sulfonate intercalated hydrotalcite, J. Hazard. Mater. 153 (2008) 911–918.

[21] W.T. Reichle, Synthesis of anionic clay minerals (mixed metal hydroxides hydrotalcite), Solid State Ionics 22 (1986) 135–141.

[22] M. Bouraada, M. Lafjah, M.S. Ouali, L.C. Demenorval, Basic dye removal from aqueous solutions by dodecylsulfate- and dodecyl benzene sulfonate-intercalated hydrotalcite, J. Hazard. Mater. 153 (2008) 911–918.

[23] L. Pesic, S. Salipurovic, V. Markovic, D. Vuselic, W. Kagunya, W. Jones, Thermal characteristics of a synthetic hydrotalcite-like material, J. Mater. Chem. 2 (1992) 1069–1073.

[24] F. Bruna, R. Celis, I. Pavlovic, C. Barriga, J. Cornejo, M.A. Ulibarri, Layered double hydroxides as adsorbents and carriers of the herbicide (4-chloro-2-methylphenoxy)acetic acid (MCPA): Systems Mg–Al, Mg–Fe and Mg–Al–Fe, J. Hazard. Mater. 168 (2009) 1476–1481.

[25] H. Zhao, K.L. Nagy, Dodecyl sulfate–hydrotalcite nanocomposites for trapping chlorinated organic pollutants in water, J. Colloid Interface Sci. 274 (2004) 613–624.

[26] B. Wang, H. Zhang, D.G. Evans, X. Duan, Surface modification of layered double hydroxides and incorporation of hydrophobic organic compounds, Mater. Chem. Phys. 92 (2005) 190–196.

[27] O.W. Perez-Lopez, A. Senger, N.R. Marcilio, M.A. Lansarin, Effect of composition and thermal pretreatment on properties of Ni–Mg–Al catalysts for CO_2 reforming of methane, Appl. Catal., A 303 (2006) 234–244.

[28] R.P. Han, Y.F. Wang, P. Han, J. Yang, Y.S. Lu, Removal of methylene blue from aqueous solution by chaff in batch mode, J. Hazard. Mater. 137 (2006) 550–557.

[29] Y. Zhou, P. Lu, J. Lu, Application of natural biosorbent and modified peat for bisphenol a removal from aqueous solutions, Carbohydr. Polym. 88 (2012) 502–508.

[30] P.C. Pavan, E.L. Crepaldi, G.A. Gomes, J.B. Valim, Adsorption of sodium dodecylsulfate on a hydrotalcite-like compound. Effect of temperature, pH and ionic strength, Colloids. Surf., A 154 (1999) 399–410.

[31] Y. Elmouzdahir, A. Elmchaouri, R. Mahboub, A. Gil, S.A. Korili, Equilibrium modeling for the adsorption of methylene blue from aqueous solutions on activated clay minerals, Desalination 250(1) (2009) 335–338.
[32] S.K. Theydan, M.J. Ahmed, Adsorption of methylene blue onto biomass-based activated carbon by $FeCl_3$ activation: Equilibrium, kinetics, and thermodynamic studies, J. Anal. Appl. Pyrol. 97 (2012) 116–122.
[33] H. Zaghouane-Boudiaf, M. Boutahala, Adsorption of 2,4,5-trichlorophenol by organo-montmorillonites from aqueous solutions: Kinetics and equilibrium studies, J. Chem. Eng. 170 (2011) 120–126.
[34] S.Y. Lagergren, Zur theorie der sogenannten adsorption geloester stoffe (On the theory of so-called adsorption of solutes), K. Sven. Vetenskapsakad. Handl. 24 (1898) 1–39.
[35] Y.S. Ho, G. McKay, Pseudo-second-order model for sorption processes, Process Biochem. 34 (1999) 451–465.
[36] R.S. Juang, M.L. Chen, Application of the Elovich equation to the kinetics of metal sorption with solvent-impregnated resins, Ind. Eng. Chem. Res. 36 (1997) 813–820.
[37] S.R. Taffarel, J. Rubio, Adsorption of sodium dodecyl benzene sulfonate from aqueous solution using a modified natural zeolite with CTAB, Miner. Eng. 23 (10) (2010) 771–779.
[38] W.J. Weber, J.C. Morris, Kinetics of adsorption on carbon from solution, J. Sanitary Eng. Div. American Society of Civil Engineers 89 (1963) 31–60.
[39] C.H. Giles, T.H. MacEwan, S.N. Nakhwa, D. Smith, J. Chem. Soc. 111 (1960) 3973.
[40] X. Wang, F. Liu, L. Lu, S. Yang, Y. Zhao, L. Sun, S. Wang, Individual and competitive adsorption of Cr(VI) and phosphate onto synthetic Fe–Al hydroxides, Colloids Surf., A 423 (2013) 42–49.
[41] W. Wang, J. Zhou, G. Achari, J. Yu, W. Cai, Cr(VI) removal from aqueous solutions by hydrothermal synthetic layered double hydroxides: Adsorption performance, coexisting anions and regeneration studies, Colloid Surf. 457 (2014) 33–40.
[42] S. Kaneko, M. Ogawa, Effective concentration of dichromate anions using layered double hydroxides from acidic solutions, Appl. Clay Sci. 75–76 (2013) 109–113.
[43] Y.X. Zhang, X.D. Hao, M. Kuang, H. Zhao, Z.Q. Wen, Preparation, characterization and dye adsorption of Au nanoparticles/ZnAl layered double oxides nanocomposites, Appl. Surf. Sci. 283 (2013) 505–512.
[44] C. Zhang, S. Yang, H. Chen, H. He, C. Sun, Adsorption behavior and mechanism of reactive brilliants red X-3B in aqueous solution over three kinds of hydrotalcite-like LDHs, Appl. Surf. Sci. 301 (2014) 329–337.
[45] N. Schouten, L.G.J. van der Ham, G-J.W. Euverink, A.B. de Haan, Selection and evaluation of adsorbents for the removal of anionic surfactants from laundry rinsing water, Water Res. 41 (2007) 4233–4241.
[46] I. Langmuir, The constitution and fundamental properties of solids and liquids. Part I. Solids, J. Am. Chem. Soc. 38 (1916) 2221–2295.
[47] F.H. Freundlich, Über die adsorption in lösungen (adsorption in solution), Z. Phys. Chem. 57 (1906) 384–470.
[48] R. Sips, On the structure of a catalyst surface, J. Chem. Phys. 16 (1948) 490–495.
[49] S. Canzano, P. Iovino, S. Salvestrini, S. Capasso, Comment on "Removal of anionic dye Congo red from aqueous solution by raw pine and acid-treated pine cone powder as adsorbent: Equilibrium, thermodynamic, kinetics, mechanism and process design", Water Res. 46 (2012) 4314–4315.
[50] S. Dawood, T.K. Sen, Author's responses to the comment by Canzano et al. and also corrigendum to "Removal of anionic dye Congo red from aqueous solution by raw pine and acid-treated pine cone powder as adsorbent: Equilibrium, thermodynamic, kinetics, mechanism and process design" published in Water Research, vol. 46, pp. 1933–1946, 2012, Water Res. 46 (2012) 4316–4317.
[51] M.I. Bautista-Toledo, J.D. Méndez-Diaz, M. Sanchez-Polo, J. Rivera-Utrilla, M.A. Ferro-Garcia, Adsorption of sodium dodecylbenzenesulfonate on activated carbons: Effects of solution chemistry and presence of bacteria, J. Colloid Interface Sci. 317 (2008) 11–17.
[52] D.C. Rodríguez-Sarmiento, J.A. Pinzón-Bello, Adsorption of sodium dodecylbenzene sulfonate on organophilic bentonites, Appl. Clay Sci. 18 (2001) 173–181.
[53] E. Fu, P. Somasundaran, C. Maltesh, Hydrocarbon and alcohol effects on sulfonate adsorption on alumina, Colloids Surf., A 112(1) (1996) 55–62.
[54] U. Ozdemir, B. Ozbay, S. Veli, S. Zor, Modeling adsorption of sodium dodecyl benzene sulfonate (SDBS) onto polyaniline (PANI) by using multi linear regression and artificial neural networks, J. Chem. Eng. 178 (2011) 183–190.